

Refine-IQA: Multi-Stage Reinforcement Finetuning For Perceptual Image Quality Assessment

Ziheng Jia, Jiaying Qian, Zicheng Zhang, Zijian Chen, Xiongkuo Min[†]

Shanghai Jiaotong University

[†]Corresponding author.

<https://github.com/jzhws/VisualQualityAssessment-RL-Trainer>

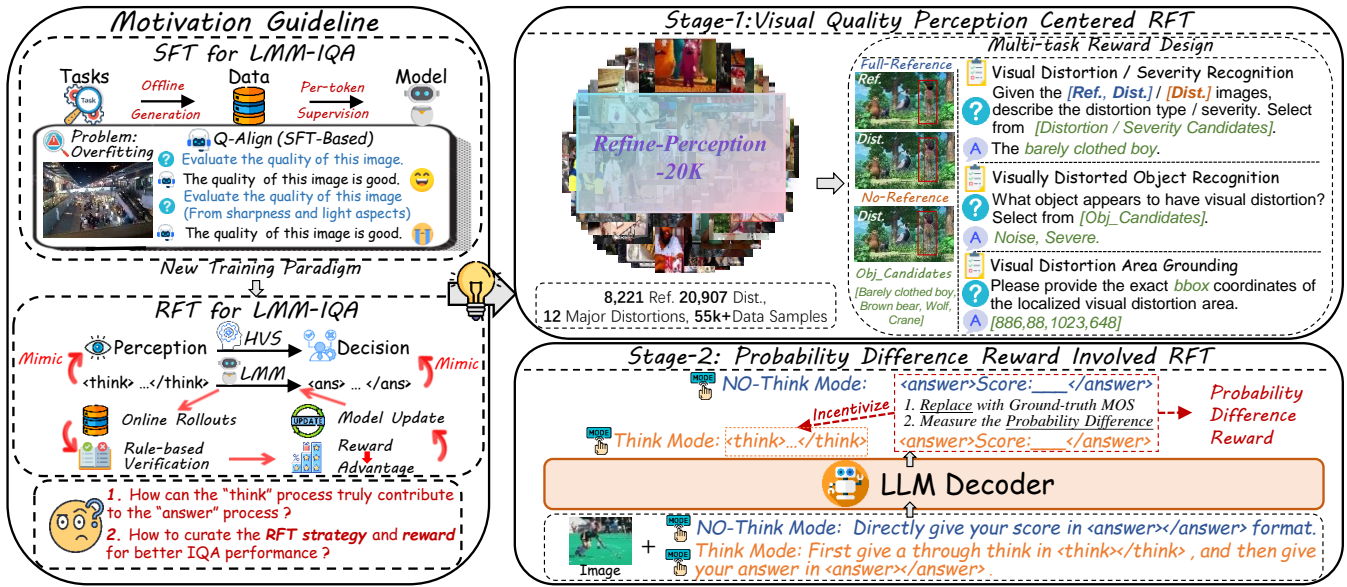


Figure 1: Overview of the *Refine-IQA*. Our primary motivation is to **curate an RFT framework that incorporates an effective “think” process, meanwhile optimizing the IQA performance**. To address these issues, we curate the *Refine-IQA*. *Stage-1* enhances the model’s inherent visual quality perception by training on the *Refine-Perception-20K* dataset with the multi-task reward system. *Stage-2* training incentivizes the “think” process through the involvement of the probability difference reward.

Abstract

Reinforcement fine-tuning (RFT) is a proliferating paradigm for LMM training. Analogous to high-level reasoning tasks, RFT is similarly applicable to low-level vision domains, including image quality assessment (IQA). Existing RFT-based IQA methods typically use rule-based output rewards to verify the model’s rollouts but provide no specific supervision for the “think” process, leaving its correctness and efficacy uncontrolled. Furthermore, these methods typically finetune directly on downstream IQA tasks without explicitly enhancing the model’s native low-level visual quality perception, which may constrain its performance upper bound. In response to these gaps, we propose a multi-stage RFT framework for IQA (**Refine-IQA**). In *Stage-1*, we build the **Refine-Perception-20K** dataset (with 12 main distortions, 20,907 locally-distorted images, and over 55K RFT samples) and design multi-task reward functions to strengthen the model’s visual quality perception. In *Stage-2*, targeting the quality scoring task, we introduce a **probability difference reward involved strategy** for “think” process supervision. The resulting **Refine-IQA Series Models** achieve outstanding performance on both perception and scoring tasks—and,

notably, our paradigm activates a robust “think” (quality-interpreting) capability that also attains exceptional results on the corresponding quality interpreting benchmark.

Introduction

Critic-model-free reinforcement learning (RL) algorithms such as *REINFORCE Leave-One-Out (RLOO)* (Ahmadian et al. 2024) and *Group Relative Policy Optimization (GRPO)* (Shao et al. 2024) have given rise to more efficient reinforcement finetuning (RFT) paradigms. These approaches utilize the model’s reward across a group of sampled outputs (rollouts) to construct intra-group advantages, thereby directly guiding the policy gradient and minimizing the dependence on label-intensive offline instruction data annotations. Consequently, this paradigm has seen widespread use in high-level large language model (LLM) and large multi-modal model (LMM) reasoning tasks such as mathematical reasoning (Shao et al. 2024; Ren et al. 2025; Wang et al. 2025a), code generation (Wang et al. 2025b), and image/video understanding (Yu et al. 2025a; Huang et al. 2025;

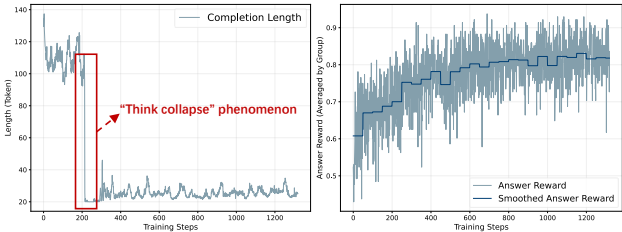


Figure 2: The visualization of the “think collapse”.

Li et al. 2025b). Likewise, it exhibits considerable promise in the low-level vision domain, with one prominent application being perceptual image quality assessment (IQA).

Most existing LMM-IQA works focus on supervised fine-tuning (SFT), explicitly **teaching** the model to enhance its visual-quality assessment capability using offline-annotated data. A major drawback of SFT is its tendency to cause **overfitting**, compromising the model’s versatility and its adherence to complex instructions. One example is depicted in the upper left of Fig. 1. Introducing RFT substantially mitigates overfitting, enables unrestrained policy exploration, and raises the upper bound of IQA performance. These merits make it a new training paradigm for this field.

The prevalent “think-answer” output paradigm of LLMs in RFT is also applicable to the IQA domain. According to the classic “perception-decision” mechanism (Mazurek et al. 2003) in the human visual system (HVS)—where the process of “perceiving visual quality features (perception)” followed by “producing a quantitative quality score (decision)” can be viewed as a close analogue to the “think-answer” process. Specifically, the LMM generates the **interpretation** of the input image’s visual quality along with its reasoning when “thinking”; subsequently, it outputs the quantitative score prediction, aligned with the image’s subjective mean opinion score (MOS) when “answering”. At this juncture, a natural question arises: *How can we ensure that the “think” process in RFT for IQA is genuinely reliable and effective?*

Unlike high-level reasoning tasks, low-level image quality perception is an **implicit, intuition-based** process. Firstly, humans do not follow a pre-defined “think” pathway when judging image visual quality. Moreover, we have surprisingly observed a “**think collapse**” phenomenon in standard *GRPO* training on the quality scoring task with rule-based outcome reward: **as the training progresses, the length of the “think” process rapidly collapses, while the model’s quality-scoring performance continues to improve (visualized in Fig. 2)**. The above findings and analysis underscore two primary technical challenges: (1) In IQA tasks, supervising the “think” process through a predefined, rule-based process reward model (PRM) is challenging. (2) Without proper reward supervision, the “think” process in the quality scoring task deteriorates over time, contributing minimally to the final decision. Moreover, we hypothesize that the “think” process serves as a **visual quality perception recalibration**, facilitating fine-grained **visual quality interpretation**. Therefore, effectively leveraging this side-effect remains a critical focus of our research.

Motivated by these challenges, we propose a **multi-stage**

reinforcement fine-tuning paradigm for constructing LMM with *refined IQA* expertise (***Refine-IQA***). The overview is shown in Fig. 1. Our core contributions are as follows:

1. We construct the **Refine–Perception–20K** dataset, the **first** RFT dataset meticulously for enhancing LMM’s **native visual quality perception**. It spans 12 primary distortion categories and comprises over 20,000 images from diverse scene contexts, each containing different *synthetic* and *localized* visual distortions. To guarantee data quality, we implement a *human-in-the-loop data scrutiny* that verifies both the semantic consistency and the perceptual clarity of the data.
2. We propose an efficient, multi-stage RFT strategy for IQA-expert LMM. Building on the *Refine-Perception-20K* dataset, we implement a multi-task reward scheme that comprehensively enhances the model’s sensitivity to low-level visual distortions (*Stage-1*). Subsequently, for the quality-decision (scoring) task, we introduce a **probability difference reward involved** strategy that implicitly supervises the “think” process by measuring the difference in ground-truth output probabilities between the “think” and “no think” modes (*Stage-2*).
3. Leveraging the curated datasets and training strategy, we develop the *Refine-IQA Series Models*, which demonstrate robust performance on quality scoring tasks across 6 IQA datasets with varied scenarios. Furthermore, these models excel in qualitative quality interpretation: with just about 13K images for quality-scoring RFT, they perform competitively with large-scale SFT-based LMMs on the quality interpretation task.

Related Works

LMM for IQA

Studies have already leveraged LMMs for IQA tasks. *Q-Align* (Wu et al. 2024c) lays the foundation of the LMM-based quality scoring using the log-probability estimation strategy. *Compare2Score* (Zhu et al. 2024) tackles subjective label scarcity using pairwise preference relationships as pseudo-labels. *Q-Instruct* (Wu et al. 2024b) and *Aestexpert* (Huang et al. 2024) pioneer in training LMMs with qualitative image quality interpretation capabilities in image technical and aesthetics quality assessment, respectively. *Co-instruct* (Wu et al. 2024d) and *DepictQA* (You et al. 2024b,a) focus on image pair quality analysis tasks.

While these approaches effectively address downstream IQA tasks, they share a common limitation: being entirely trained on SFT, they experience substantial degradation in multi-task versatility and adherence to complex instructions.

RFT for IQA

Recently, research has begun to involve RL strategies for LMM-IQA. *Q-Insight* (Li et al. 2025a) employs the standard rule-based outcome reward for multi-task RFT. *Q-Ponder* (Cai et al. 2025) follows the “Cold-start to RL” workflow to construct a comprehensive training pipeline.

Although these works represent valuable advances, they share some limitations. First, they do not explicitly enhance

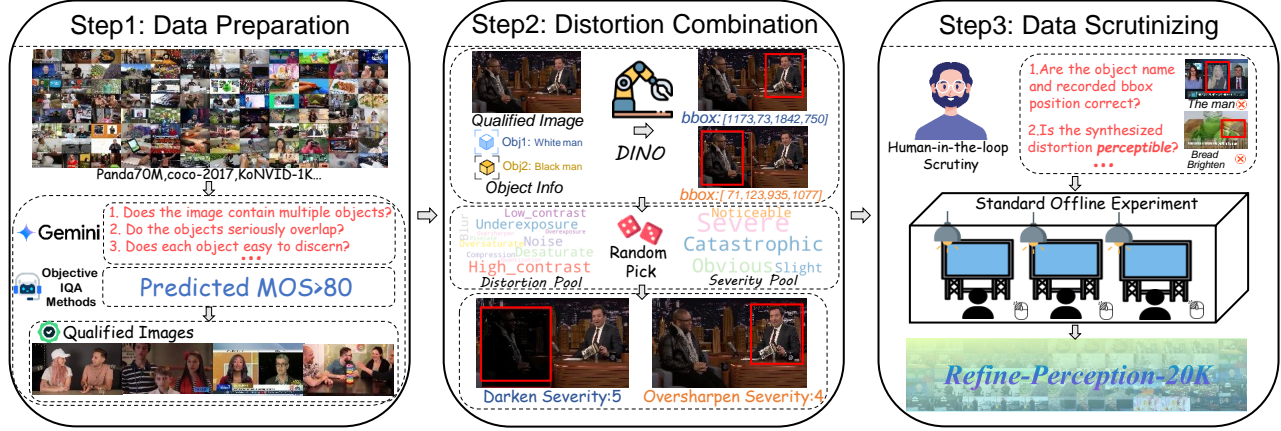


Figure 3: The construction pipeline of the *Refine-Perception-20K* dataset.

the LMM’s visual quality perception; instead, they directly fine-tune the model on downstream tasks — potentially constraining its performance ceiling. More critically, these models fail to incorporate reward supervision for the “think” process, thereby reducing it to an ancillary output. These shortcomings present insights for our work.

The Refine-IQA

To design an RFT framework that supports effective “think” process and empowers the LMM with refined IQA performance, a key focus is enhancing the model’s native ability to perceive low-level visual quality features - specifically, its ability to **identify fundamental visual distortion types, severity, and location**. Simultaneously, it is also crucial to establish a reward scheme that **bridges the gap between the “think” and “answer” processes**. In response to this, we develop *Refine-IQA*, a comprehensive RFT paradigm.

Visual Quality Perception Centered RL

In *Stage-1*, we have constructed the *Refine-Perception-20K*, a dataset of 20,907 images, encompassing 12 distortion types and 5 levels of distortion severity. The construction pipeline is demonstrated in Fig. 3. The detailed statistical information is recorded in *Supplementary Material (Supp.)*.

Dataset Construction Pipeline The dataset construction commences with data preparation. To ensure that the source image pool enables the identification of multiple objects, the data source needs to contain relatively complex semantic content. Therefore, we extract keyframes from the video datasets *LSVQ* (Ying et al. 2021) and *Panda-70M* (Chen et al. 2024) and select images from the *COCO* object-detection dataset (Lin et al. 2014), resulting in over 100,000 images across varying resolutions and contexts. To mitigate the effects of inherent visual distortions, three state-of-the-art objective IQA models—*Q-Align* (Wu et al. 2024c), *DBCNN* (Zhang et al. 2020), and *Hyper-IQA* (Su et al. 2020)—are employed to compute the quality score for each image, with only those with all three scores above 80 retained. Next, we utilize *Gemini-2.5-PRO* (Team et al. 2024)

to filter images containing at least two distinct semantic objects, recording a concise phrase-level description for each identified object. This process yields 8,221 qualified images along with their semantic object information.

Subsequently, we employ *DINO* (Ren et al. 2024) to perform object detection on the qualified images using the recorded information. For each source image, a single bounding box (bbox)—specified by its top-left (x_{TL}, y_{TL}) and bottom-right (x_{BR}, y_{BR}) coordinates—is generated for each annotated object. This procedure results in over 30K marked images, each containing exactly one bbox. We then randomly apply distortions of varying severity to the bbox regions. The **distortion pool** comprise *blur*, *noise*, *compression*, *overexposure*, *underexposure*, *high contrast*, *low contrast*, *oversaturate*, *desaturate*, *oversharpen*, *pixelate*, and *quantization*, and the **severity candidates** encompass *slight*, *just noticeable*, *relatively obvious*, *severe*, and *very severe*. We partially adopt the distortion combination method from *DepictQA-V2* (You et al. 2024a), which is detailed in *Supp.*.

As the perceptibility of synthetic distortions depends on both content and visual characteristics, human-in-the-loop scrutiny is essential. Therefore, we conduct a subjective experiment in a standard laboratory environment. Human experts are instructed to exclude any images where the bbox content fails to match the description or where the added distortion is not perceptible. The subjective experiment settings are given in *Supp.*. Finally, we extract 1,500 images for test (denoted as *Refine-Perception-20K-test*), with the remaining part used for training (*Refine-Perception-20K-train*). The distortion distribution in both parts is kept consistent.

Multi-Task Reward Design We employ *Qwen2.5-VL-7B* (Bai et al. 2025) as the base model. Considering that it has already obtained inherent capability for low-level visual perception (i.e., the ability to recognize commonly-seen distortion types), our objective is to **calibrate** and **refine** such ability through RFT. Thus, we employ a multi-task, rule-based reward schema in conjunction with standard *GRPO* for RFT. Here we define the fundamental sub-tasks:

- 1. Visual Distortion Type / Severity Recognition** To ensure verifiability, this task is formulated as a multi-choice

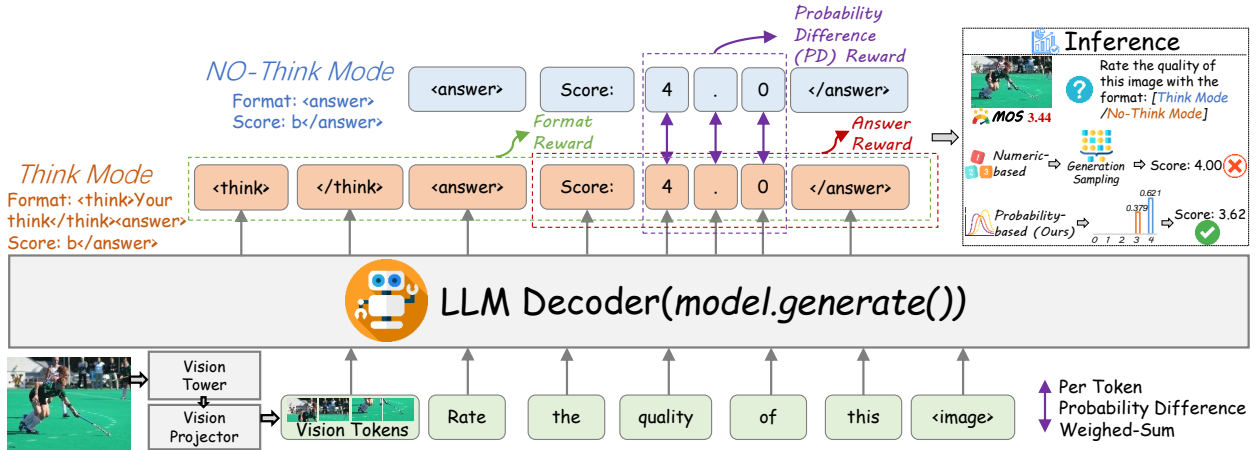


Figure 4: The model structure, our inference method, and the illustration of the PD reward involved RL strategy.

(single-answer) problem. The distortion and severity pool serve as candidate choice sets; the model receives a reward 1 only if its output matches the correct answer.

2. **Visually Distorted (Semantic) Object Recognition** Also arranged as a multi-choice task. Candidate answers are drawn from the recorded semantic objects of the original image. The verification rule is identical to the above.
3. **Visual Distortion Area Grounding** The model outputs the coordinates of the bbox enclosing the distortion area. The reward is computed as the Intersection-over-Union (*IoU*) between the predicted and ground-truth bboxes.

All three tasks include the “full-reference” (FR) (with the original and distorted images) and “no-reference” (NR) (only with the distorted image) sub-tasks (examples are shown in the upper right of Fig. 1 and detailed in *Supp.*). Finally, we obtain over 55K RFT data samples. During training, data from all three tasks are randomly mixed.

Probability Difference Reward Involved RL

For the quality-decision (scoring) task, the primary focus is to ensure that the “think” process is genuinely effective while optimizing its alignment with the ground-truth MOS. Accordingly, we propose the *probability difference reward involved* RFT strategy (depicted in detail in Fig. 4).

The “Think Collapse” Phenomenon We use the outcome answer reward r_{ans} and standard *GRPO* setting for the quality scoring task. The r_{ans} is denoted as:

$$r_{\text{ans}} = 1 \quad \text{if } |\hat{s} - s| < \epsilon, \text{ otherwise } 0, \quad (1)$$

where \hat{s} and s are the predicted and ground-truth scores on a $[0, 5]$ scale, and ϵ is set to 0.5. During training, we observe the above-mentioned “think collapse” phenomenon. We provide further explanation in *Supp.*.

The Probability Difference Reward To address this issue, we introduce the *probability difference (PD) reward*, which provides implicit supervision on the “think” process.

LLMs inherently model text generation as **next-token probability prediction**. In the “think-answer” paradigm, the

increase in the probability of the ground-truth—relative to the “no-think” mode—signals a greater contribution from the “think” process. This motivates our use of the difference in ground-truth token probabilities (likelihoods) between the “think” and “no-think” modes as the reward signal. Given the ground-truth MOS with $M - 1$ decimal places (we assign $M = 2$), we set $z^{\text{think}} \in \mathbb{R}^M$ and $z^{\text{no-think}} \in \mathbb{R}^M$ as the predicted probabilities (*softmax normalization to the vocab logits*) corresponding to each digit of the ground-truth MOS under the “think” and “no-think” modes. We derive the reward for the two modes through the weighted sum of the token probability of each ground-truth MOS digit:

$$r_{\text{MODE}} = w_0 z_0^{\text{MODE}} + w_1 z_1^{\text{MODE}} + \dots + w_{M-1} z_{M-1}^{\text{MODE}}, \quad (2)$$

where the placeholder *MODE* can be replaced by *think* or *no-think*. The weights can be formulated as $w = [w_0, w_1, \dots, w_{M-1}] = [1, 0.1, \dots, 10^{1-M}]$. For the i -th rollout in one group, its probability difference reward r_{pd}^i is:

$$r_{\text{pd}}^i = \text{clip}(r_{\text{think}}^i - r_{\text{no-think}}^i, 0, 1). \quad (3)$$

Specifically, we employ two distinct prompts corresponding to the two modes to elicit rollouts. Thereafter, we replace the model’s predicted score with the ground-truth MOS (with the same digit numbers) and calculate the probability of each corresponding ground-truth token. It is important to note that the output format of the “no-think” mode is fixed, resulting in the invariant likelihoods for the ground-truth MOS tokens within each group; hence, the $r_{\text{no-think}}^i$ can be denoted as r_{ref} and r_{pd}^i can be reformulated as:

$$r_{\text{pd}}^i = \text{clip}(r_{\text{think}}^i - r_{\text{ref}}, 0, 1). \quad (4)$$

The final reward r_{final}^i is defined as the weighted sum of the answer reward r_{ans}^i (same as the setting in Eq. 1), the format reward r_{fmt}^i (the reward is 1 only if the output format follows the requirement and otherwise 0) and the r_{pd}^i :

$$r_{\text{final}}^i = \lambda_1 r_{\text{ans}}^i + \lambda_2 r_{\text{fmt}}^i + \lambda_3 r_{\text{pd}}^i \quad \text{if } r_{\text{ans}}^i = r_{\text{fmt}}^i = 1, \\ \text{otherwise } \lambda_1 r_{\text{ans}}^i + \lambda_2 r_{\text{fmt}}^i, \quad (5)$$

we set $\lambda_1 = \lambda_2 = \lambda_3 = 1$. The rationale for our reward design can be summarized as follows: Overall, the r_{pd} functions as an **incremental incentive**. When the model’s scoring accuracy for one training sample (quantified by the proportion of qualified rollouts with $r_{\text{ans}} = r_{\text{fmt}} = 1$ in one group) is low, the training concentrates on improving the accuracy. Only when accuracy is sufficiently high do rollouts with higher PD rewards provide additional advantage. This ensures correct predictions are effectively utilized, while preventing training instability.

Modifying the Gradient Policy for Quality Scoring In *GRPO*, the intra-group advantage calculation is prone to assigning negative advantages to incorrect rollouts, leading to decreased probabilities. For the quality scoring task, this may result in overly definite outputs, which impairs the generalization ability. To address this, we draw inspiration from *Q-Align* and reformulate the scoring task as a **quality level classification (distribution prediction)** task. We define the modified group-relative (with G rollouts) advantage as:

$$\hat{A}_{i,t} = \max \left[\frac{r^{(i)} - \text{mean}(\{r^{(1)}, r^{(2)}, \dots, r^{(G)}\})}{\text{std}(\{r^{(1)}, r^{(2)}, \dots, r^{(G)}\})}, 0 \right]$$

if $0 \leq |\lambda_1 r_{\text{ans}} + \lambda_2 r_{\text{fmt}}| < \lambda_1 + \lambda_2 < G$,

$$\text{otherwise } \hat{A}_{i,t} = \frac{r^{(i)} - \text{mean}(\{r^{(1)}, r^{(2)}, \dots, r^{(G)}\}) - 0.02}{\text{std}(\{r^{(1)}, r^{(2)}, \dots, r^{(G)}\})}.$$
(6)

Following techniques proposed in *DAPO* (Yu et al. 2025b), we remove the KL penalty and shift from *sample-level* averaging to *token-level* averaging in the loss processing to promote a longer “think” process. Finally, let V be an input image and q be its scoring prompt. The modified *GRPO* optimization objective is denoted as:

$$\mathcal{J}(\theta) = \mathbb{E} \left[q \sim P(Q), \{o_i\}_{i=1}^G \sim \pi_{\theta_{\text{old}}}(O | q, V) \right]$$

$$\frac{1}{\sum_{i=1}^G |o_i|} \sum_{i=1}^G \sum_{t=1}^{|o_i|} \left\{ \min \left[\rho_{i,t} \hat{A}_{i,t}, \text{clip}(\rho_{i,t}, 1 - \varepsilon, 1 + \varepsilon) \hat{A}_{i,t} \right] \right\},$$
(7)

where Q denotes the input prompt set and $\rho_{i,t}$ represents the importance sampling coefficient $\frac{\pi_{\theta}(o_{i,t} | q, V, o_{i,<t})}{\pi_{\theta_{\text{old}}}(o_{i,t} | q, V, o_{i,<t})}$. In an on-policy setting without importance sampling, this configuration mirrors a **cross-entropy optimization target with dynamic gradient weights** (the detailed proof is presented in *Supp.*). Correct rollouts of training samples that are difficult to score accurately receive higher advantages, driving the model to prioritize their optimization. If no rollout in a group is correct ($|\lambda_1 r_{\text{ans}} + \lambda_2 r_{\text{fmt}}| = G$), a negative advantage is employed to prevent training data waste and encourage exploration of alternative predictions.

Inference Method We adopt the following **probability-based expectation estimation** (shown in Fig. 4) to obtain the score \mathcal{Q} from output vocab logits in the inference stage:

$$\mathcal{Q} = \sum_{j=0}^4 j \frac{e^{\mathcal{P}_j}}{\sum_{i=0}^4 e^{\mathcal{P}_i}} + 0.5,$$
(8)

where \mathcal{P} denotes the model’s **logits** of the corresponding digit values on the output **integer part**.

The Refine-IQA Series Models

Building upon the *Refine-IQA*, we derive the *Refine-IQA Series Models*. In *Stage-1*, a single epoch training in “no-think” mode on *Refine-Perception-20K-train* produces *Refine-IQA-S1*. Subsequently, we advance to *Stage-2*, performing 3 training epochs in “think” mode on the combined dataset of *KoniQ-10K* (Hosu et al. 2020) and *SPAQ* (Fang et al. 2020) training sets (approximately 13K samples, the ground-truth MOS of all training data is uniformly scaled to the range $[0, 5)$) to produce *Refine-IQA-S2*. The training prompts design is shown in *Supp.*. All experiments are conducted on 8 NVIDIA A100 (80 GB) GPUs, with G set to 8.

Experiments

To rigorously assess the performance of the *Refine-IQA Series Models*, we perform extensive comparison experiments. Additionally, we carry out ablation studies on the critical configurations to enable more in-depth analysis.

Performance on Image Quality Perception

We evaluate the models’ visual quality perception capability using the *Refine-Perception-20K-test*. First, we partition the test data by distortion type based on their prevalence in natural scenes into two categories: **Easy** and **Hard**. We then assess the two sub-tasks: (1) **Description**: For each image, the model identifies the distortion category, the distorted semantic object, and the distortion severity from the candidate pools. A test case is deemed correct only if all three attributes are correctly chosen. We record the overall accuracy as the experimental result. (2) **Grounding**: We compute the *IoU* between the model’s predicted and the ground-truth region. Since no open-source quality perception LMM is currently available, we only compare against the base model (all models use the “no-think” mode). The results for the two tasks are shown in the Tabs. 1 and 2. They indicate that after RFT, the model exhibits significant improvements in performance on both tasks, particularly in **Hard** cases and the **Grounding** task. This suggests that, although RFT does not introduce new knowledge, it effectively guides the model to recalibrate its native visual quality perception capabilities.

Performance on Image Quality Scoring

We select in-domain (in-the-wild) IQA datasets *KoniQ (test set)*, *SPAQ (test set)*, and *LIVE-C* (Ghadiyaram and Bovik 2015), alongside out-of-domain datasets *AGIQA-3K* (Li et al. 2023) (AIGC-images), *KADID-10K* (Lin, Hosu, and Saupe 2019), and *CSIQ* (Larson and Chandler 2010) (synthetic distortions) for evaluation. We carefully search the comparison models **with open-source training code** for reproduction. Except for the *Q-Align series* and *Compare2Score*, in which we use pre-trained LMMs, all comparison models are retrained on the same training dataset as ours (for *Q-Insight*, we adopt the training setup with only the quality scoring task). The evaluation metrics are the commonly used *Pearson Linear Correlation Coefficient* (PLCC) and *Spearman Rank Correlation Coefficient* (SRCC). The results are shown in Tab. 3. The *Refine-IQA-S2* achieves excellent performance across all six datasets under both

Table 1: *Description* performance on image quality perception task on the *Refine-Perception-20K-test* (where *Comp.*, *OE*, *UE*, *OSat.*, *DSat.*, *OSharp.*, *HC*, *LC*, *Pixel.*, and *Quant.* represent *compression*, *overexposure*, *underexposure*, *oversaturation*, *desaturation*, *oversharpening*, *high contrast*, *low contrast*, *pixelation*, and *quantization*, respectively). *Advantage* denotes the performance improvement of the *Refine-IQA-S1* compared to the *base model*. [Per column: highest in **bold**.]

Table 2: *Grounding* performance on image quality perception task. [Per column: highest in **bold**.]

CATEGORIES	EASY					HARD					Overall		
Models	Blur	Noise	Comp.	OE	UE	OSat.	DSat.	OSharp.	HC	LC	Pixel.	Quant.	
Qwen2.5-VL-7B (base)	0.542	0.513	0.489	0.403	0.398	0.298	0.245	0.283	0.192	0.332	0.352	0.143	0.343
Refine-IQA-S1	0.952	0.943	0.965	0.982	0.885	0.752	0.788	0.679	0.737	0.685	0.483	0.315	0.772
Refine-IQA-S2	0.898	0.903	0.869	0.937	0.832	0.705	0.723	0.632	0.658	0.617	0.392	0.252	0.738
Advantage	0.410	0.430	0.476	0.579	0.487	0.454	0.543	0.396	0.545	0.353	0.131	0.172	0.429

Table 3: Evaluation results on image quality scoring task (*w think* and *w/o think* denote that the model turns on / off the “think” mode during evaluation. Except where specifically indicated, all other models are tested using the “no think” mode). [Per column: highest in **bold**, second in *italic*, third in underlined.]

Datasets		KONIQ		SPAQ		LIVE-C		AGIQA-3K		KADID-10K		CSIQ	
Models		SRCC	PLCC										
<i>Performance of Deep Neural Network (DNN)-Based Models</i>													
NIMA (Talebi and Milanfar 2018)		0.859	0.896	0.856	0.838	0.771	0.814	0.654	0.715	0.535	0.532	0.662	0.683
DBCNN (Zhang et al. 2020)		0.875	0.884	0.806	0.812	0.755	0.773	0.641	0.730	0.484	0.497	0.552	0.589
HyperIQA (Su et al. 2020)		0.906	0.917	0.788	0.791	0.749	0.772	0.640	0.702	0.468	0.506	0.631	0.685
MUSIQ (Ke et al. 2021)		0.919	0.914	0.863	0.868	0.830	0.789	0.630	0.722	0.556	0.575	0.642	0.698
CLIP-IQA+ (Wang, Chan, and Loy 2022)		0.895	0.909	0.864	0.866	0.805	0.832	0.685	0.736	0.654	0.653	0.695	0.710
LIQE (Zhang et al. 2023)		0.928	0.912	0.833	0.846	0.870	0.830	0.708	0.772	0.662	0.667	0.703	0.715
<i>Performance of SFT-Based Domain-Specific LMMs</i>													
Q-Align-IQA-7B (Wu et al. 2023)		0.920	0.918	0.897	0.896	0.860	0.853	0.735	0.772	0.684	0.674	0.668	0.701
Q-Align-Onealign-7B		0.933	0.930	0.915	0.908	0.868	0.872	0.758	0.801	0.712	0.725	0.683	0.715
Compare2Score-7B (Zhu et al. 2024)		0.915	0.905	0.924	0.914	0.808	0.787	0.765	0.703	0.532	0.585	0.686	0.700
<i>Performance of RL-Based Domain-Specific LMMs</i>													
Q-Insight-7B (Li et al. 2025a) (w think)		0.860	0.873	0.873	0.881	0.785	0.824	0.758	0.785	0.573	0.591	0.665	0.692
Q-Insight-7B (w/o think)		0.871	0.894	0.899	0.902	0.801	0.833	0.777	0.832	0.580	0.584	0.683	0.714
<i>Performance of Refine-IQA Series Models</i>													
Refine-IQA-S2 (w think)		0.920	0.916	0.930	0.918	0.870	0.892	0.789	0.835	0.703	0.715	0.711	0.739
Refine-IQA-S2 (w/o think)		0.938	0.924	0.927	0.921	0.860	0.885	0.798	0.841	0.698	0.702	0.724	0.758

Table 4: Evaluation results on the *O-Bench-test*. [Per column: highest in **bold**, second in *italic*, third underlined.]

Table 5: Ablation study of the effects of *Stage-1* (using the *Refine-IQA-S2* (w/o think)). **SCORING** performance is represented as the average of *SRCC* and *PLCC* on the individual dataset. The **INTERPRETING** performance is reported as the performance on the *Technical* (*Tech.*) and *Overall* dimensions. [Per column: highest in **bold**.]

TRAIN	SCORING				INTERPRET	
	<i>KoniQ</i>	<i>AGIQA</i>	<i>SPAQ</i>	<i>KADID</i>	<i>Tech.</i>	<i>Overall</i>
w/o <i>Stage-1</i>	0.916	0.815	0.920	0.671	80.10%	79.85%
w <i>Stage-1</i>	0.931	0.817	0.924	0.709	81.27%	80.78%

“think” and “no-think” modes. Notably, the negligible performance gap between the two modes (compared to *Q-Insight*) underscores the effectiveness of the “think” process.

Performance on Image Quality Interpreting

As previously discussed, we believe that developing an effective “think” process in the quality scoring task RFT can improve the LMM’s performance in quality interpretation (further explained in *Supp.*). To validate this, we choose the *Q-bench-test* (Wu et al. 2024a) (with 1,495 multi-choice (single answer) questions). Here, we select the latest open-sourced and proprietary general LMMs, along with some high-performing IQA-LMMs for comparison. All models are evaluated using the *model.generate()* mode with *greedy search* to ensure reproducibility.

The experiment results are shown in Tab.4, from which we have some critical observations: (1) After the perception-centered RFT *Stage-1*, the *Refine-IQA-S1* already demonstrates improved performance. (2) The *Refine-IQA-S2* achieves substantial gains under both “think” and “no-think” modes (particularly in the *Technical* dimension)—significantly outperforming general LMMs and nearly matching the fine-tuned base model (with SFT) using the *Q-Pathway-200K* (*Q-Instruct*) (Wu et al. 2024b). This indicates that the “think” process in *Stage-2* RFT further refines the model’s visual quality interpreting ability.

Ablation Study

The Effects of *Stage-1* Training We alternatively remove the *Stage-1* training, with all other training and evaluation settings kept consistent. The performance of this ablation experiment is shown in Tab. 5.

The results demonstrate that the *Stage-1* training positively optimizes the model’s performance on both scoring and interpreting tasks, highlighting the importance of enhancing the model’s inherent quality perception capabilities.

***Stage-2* Attributes Ablation Study** We ablate key attributes in *Stage-2*, while keeping other settings the same. The ablation results are presented in Tab. 6. Here, we present some key findings: (1) After removing the *PD* reward, the model exhibits the “think collapse”, and performance on the quality interpreting task significantly decreases, highlighting that reward supervision for the “think” process is essential for ensuring its effectiveness. (2) The *PM* strategy is necessary for successfully applying the probability-based inference method for scoring. Furthermore, our experimen-

Table 6: Ablation study of *Stage-2* attributes (using the *Refine-IQA-S2* (w/o think)). *PD* denotes the probability difference reward and *PM* represents the policy gradient modification. *Num.* and *Prob.* represent the numeric-based and probability-based inference strategy in the scoring task. The inference method for the interpreting task is the same as the above-mentioned. [Per column: highest in **bold**.]

TRAIN	INFERENCE	SCORING				INTERPRET	
		<i>KoniQ</i>	<i>AGIQA</i>	<i>SPAQ</i>	<i>KADID</i>	<i>Tech.</i>	<i>Overall</i>
<i>PD</i>	<i>PM</i>	<i>Num.</i>	<i>Prob.</i>	0.928	0.815	0.930	0.702
✗	✓	✗	✓	0.735	0.629	0.762	0.487
✓	✗	✗	✓	0.912	0.808	0.907	0.691
✓	✓	✓	✗	0.931	0.817	0.924	0.709
						81.27%	80.78%

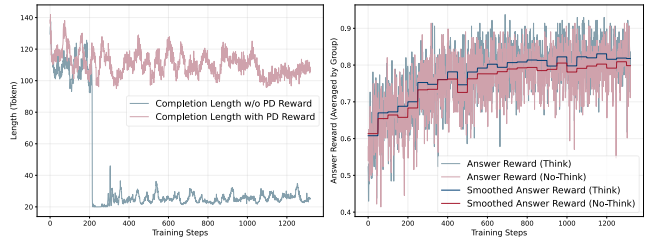


Figure 5: *Left*: The *Stage-2* completion length with / w/o PD reward. *Right*: The *Stage-2* group averaged answer reward of “think” and “no-think” modes during training.

tal setup maintains the optimal performance in all ablation settings, validating its rationality.

In addition, we present visualizations of some training ablation details in Fig. 5. As shown on the left, the integration of the *PD reward* effectively suppresses the “think collapse” phenomenon, further validating its role in incentivizing the “think” process. The right figure demonstrates that, in the absence of specific optimization for the “no-think” mode output, its output accuracy still increases simultaneously with the “think” mode. This observation justifies our decision to exclude dedicated model optimization for the “no-think” mode when calculating the PD reward.

Conclusion

In this paper, we propose the *Refine-IQA*, an RFT framework that focuses on enhancing the LMM’s perception of low-level visual quality (*Stage-1*) and incentivizing the model’s effective “think” capability for IQA (*Stage-2*). In *Stage-1*, we construct the *Refine-Perception-20K* dataset and a multi-task reward scheme. In *Stage-2*, we introduce the *probability difference reward* for the “think” process along with *gradient policy modification*. After training, we obtain the *Refine-IQA Series Models*, which achieve excellent performance on both quality perception and scoring tasks. Additionally, we validate the model’s “think” capability in quality interpretation tasks. With only approximately 13K scoring labels for RFT, we can trigger the model’s “think” capability, enabling its performance to rival that of LMM developed through large-scale SFT. Our work provides compelling insights for developing **efficient visual quality assessment agents** that are both **labeling friendly** and **functionally robust**.

References

Achiam, J.; Adler, S.; Agarwal, S.; Ahmad, L.; Akkaya, I.; Aleman, F. L.; Almeida, D.; Altenschmidt, J.; Altman, S.; Anadkat, S.; et al. 2023. Gpt-4 technical report. *arXiv preprint arXiv:2303.08774*.

Ahmadian, A.; Cremer, C.; Gallé, M.; Fadaee, M.; Kreutzer, J.; Pietquin, O.; Üstün, A.; and Hooker, S. 2024. Back to basics: Revisiting reinforce style optimization for learning from human feedback in llms. *arXiv preprint arXiv:2402.14740*.

Anthropic, T. 2025. Claude 3.7 sonnet and claude code.

Bai, S.; Chen, K.; Liu, X.; Wang, J.; Ge, W.; Song, S.; Dang, K.; Wang, P.; Wang, S.; Tang, J.; et al. 2025. Qwen2. 5-VL Technical Report. *arXiv preprint arXiv:2502.13923*.

Cai, Z.; Zhang, J.; Yuan, X.; Jiang, P.-T.; Chen, W.; Tang, B.; Yao, L.; Wang, Q.; Chen, J.; and Li, B. 2025. Q-Ponder: A Unified Training Pipeline for Reasoning-based Visual Quality Assessment. *arXiv preprint arXiv:2506.05384*.

Chen, T.-S.; Siarohin, A.; Menapace, W.; Deyneka, E.; Chao, H.-w.; Jeon, B. E.; Fang, Y.; Lee, H.-Y.; Ren, J.; Yang, M.-H.; et al. 2024. Panda-70m: Captioning 70m videos with multiple cross-modality teachers. In *CVPR*, 13320–13331.

Fang, Y.; Zhu, H.; Zeng, Y.; Ma, K.; and Wang, Z. 2020. Perceptual quality assessment of smartphone photography. In *Proceedings of the IEEE/CVF conference on computer vision and pattern recognition*, 3677–3686.

Ghadiyaram, D.; and Bovik, A. C. 2015. Massive online crowdsourced study of subjective and objective picture quality. *IEEE TIP*, 25(1): 372–387.

Hosu, V.; Lin, H.; Sziranyi, T.; and Saupe, D. 2020. KonIQ-10k: An ecologically valid database for deep learning of blind image quality assessment. *IEEE TIP*, 29: 4041–4056.

Huang, W.; Jia, B.; Zhai, Z.; Cao, S.; Ye, Z.; Zhao, F.; Xu, Z.; Hu, Y.; and Lin, S. 2025. Vision-r1: Incentivizing reasoning capability in multimodal large language models. *arXiv preprint arXiv:2503.06749*.

Huang, Y.; Sheng, X.; Yang, Z.; Yuan, Q.; Duan, Z.; Chen, P.; Li, L.; Lin, W.; and Shi, G. 2024. AesExpert: Towards Multi-modality Foundation Model for Image Aesthetics Perception. *arXiv preprint arXiv:2404.09624*.

Ke, J.; Wang, Q.; Wang, Y.; Milanfar, P.; and Yang, F. 2021. MUSICQ: Multi-Scale Image Quality Transformer. In *ICCV*, 5148–5157.

Larson, E. C.; and Chandler, D. M. 2010. Most apparent distortion: full-reference image quality assessment and the role of strategy. *Journal of electronic imaging*, 19(1): 011006–011006.

Li, B.; Zhang, Y.; Guo, D.; Zhang, R.; Li, F.; Zhang, H.; Zhang, K.; Li, Y.; Liu, Z.; and Li, C. 2024. Llava-onevision: Easy visual task transfer. *arXiv preprint arXiv:2408.03326*.

Li, C.; Zhang, Z.; Wu, H.; Sun, W.; Min, X.; Liu, X.; Zhai, G.; and Lin, W. 2023. AGIQA-3K: An Open Database for AI-Generated Image Quality Assessment. *arXiv:2306.04717*.

Li, W.; Zhang, X.; Zhao, S.; Zhang, Y.; Li, J.; Zhang, L.; and Zhang, J. 2025a. Q-insight: Understanding image quality via visual reinforcement learning. *arXiv preprint arXiv:2503.22679*.

Li, X.; Yan, Z.; Meng, D.; Dong, L.; Zeng, X.; He, Y.; Wang, Y.; Qiao, Y.; Wang, Y.; and Wang, L. 2025b. Videochat-r1: Enhancing spatio-temporal perception via reinforcement fine-tuning. *arXiv preprint arXiv:2504.06958*.

Lin, H.; Hosu, V.; and Saupe, D. 2019. KADID-10k: A large-scale artificially distorted IQA database. In *QoMEX*, 1–3.

Lin, T.-Y.; Maire, M.; Belongie, S.; Hays, J.; Perona, P.; Ramanan, D.; Dollár, P.; and Zitnick, C. L. 2014. Microsoft coco: Common objects in context. In *European conference on computer vision*, 740–755. Springer.

Mazurek, M. E.; Roitman, J. D.; Ditterich, J.; and Shadlen, M. N. 2003. A role for neural integrators in perceptual decision making. *Cerebral cortex*, 13(11): 1257–1269.

Ren, T.; Chen, Y.; Jiang, Q.; Zeng, Z.; Xiong, Y.; Liu, W.; Ma, Z.; Shen, J.; Gao, Y.; Jiang, X.; et al. 2024. Dino-x: A unified vision model for open-world object detection and understanding. *arXiv preprint arXiv:2411.14347*.

Ren, Z.; Shao, Z.; Song, J.; Xin, H.; Wang, H.; Zhao, W.; Zhang, L.; Fu, Z.; Zhu, Q.; Yang, D.; et al. 2025. Deepseek-prover-v2: Advancing formal mathematical reasoning via reinforcement learning for subgoal decomposition. *arXiv preprint arXiv:2504.21801*.

Shao, Z.; Wang, P.; Zhu, Q.; Xu, R.; Song, J.; Bi, X.; Zhang, H.; Zhang, M.; Li, Y.; Wu, Y.; et al. 2024. Deepseekmath: Pushing the limits of mathematical reasoning in open language models. *arXiv preprint arXiv:2402.03300*.

Su, S.; Yan, Q.; Zhu, Y.; Zhang, C.; Ge, X.; Sun, J.; and Zhang, Y. 2020. Blindly Assess Image Quality in the Wild Guided by a Self-Adaptive Hyper Network. In *CVPR*.

Talebi, H.; and Milanfar, P. 2018. NIMA: Neural Image Assessment. *IEEE TIP*.

Team, G.; Georgiev, P.; Lei, V. I.; Burnell, R.; Bai, L.; Gulati, A.; Tanzer, G.; Vincent, D.; Pan, Z.; Wang, S.; et al. 2024. Gemini 1.5: Unlocking multimodal understanding across millions of tokens of context. *arXiv preprint arXiv:2403.05530*.

Wang, J.; Chan, K. C. K.; and Loy, C. C. 2022. Exploring CLIP for Assessing the Look and Feel of Images.

Wang, P.; Bai, S.; Tan, S.; Wang, S.; Fan, Z.; Bai, J.; Chen, K.; Liu, X.; Wang, J.; Ge, W.; et al. 2024. Qwen2-vl: Enhancing vision-language model’s perception of the world at any resolution. *arXiv preprint arXiv:2409.12191*.

Wang, W.; Gao, Z.; Chen, L.; Chen, Z.; Zhu, J.; Zhao, X.; Liu, Y.; Cao, Y.; Ye, S.; Zhu, X.; et al. 2025a. Visualprm: An effective process reward model for multimodal reasoning. *arXiv preprint arXiv:2503.10291*.

Wang, Y.; Yang, L.; Tian, Y.; Shen, K.; and Wang, M. 2025b. Co-evolving llm coder and unit tester via reinforcement learning. *arXiv preprint arXiv:2506.03136*.

Wu, H.; Zhang, Z.; Zhang, E.; Chen, C.; Liao, L.; Wang, A.; Li, C.; Sun, W.; Yan, Q.; Zhai, G.; and Lin, W. 2024a.

Q-Bench: A Benchmark for General-Purpose Foundation Models on Low-level Vision. In *ICLR*.

Wu, H.; Zhang, Z.; Zhang, E.; Chen, C.; Liao, L.; Wang, A.; Xu, K.; Li, C.; Hou, J.; Zhai, G.; et al. 2024b. Q-instruct: Improving low-level visual abilities for multi-modality foundation models. In *CVPR*, 25490–25500.

Wu, H.; Zhang, Z.; Zhang, W.; Chen, C.; Liao, L.; Li, C.; Gao, Y.; Wang, A.; Zhang, E.; Sun, W.; et al. 2023. Q-align: Teaching Lmms for visual scoring via discrete text-defined levels. *arXiv preprint arXiv:2312.17090*.

Wu, H.; Zhang, Z.; Zhang, W.; Chen, C.; Liao, L.; Li, C.; Gao, Y.; Wang, A.; Zhang, E.; Sun, W.; et al. 2024c. Q-ALIGN: teaching LMMs for visual scoring via discrete text-defined levels. In *ICML*, 54015–54029.

Wu, H.; Zhu, H.; Zhang, Z.; Zhang, E.; Chen, C.; Liao, L.; Li, C.; Wang, A.; Sun, W.; Yan, Q.; et al. 2024d. Towards open-ended visual quality comparison. In *ECCV*, 360–377.

Ye, Q.; Xu, H.; Ye, J.; Yan, M.; Hu, A.; Liu, H.; Qian, Q.; Zhang, J.; and Huang, F. 2024. mplug-owl2: Revolutionizing multi-modal large language model with modality collaboration. In *CVPR*, 13040–13051.

Ying, Z.; Mandal, M.; Ghadiyaram, D.; and Bovik, A. 2021. Patch-vq: ‘patching up’the video quality problem. In *CVPR*, 14019–14029.

You, Z.; Gu, J.; Li, Z.; Cai, X.; Zhu, K.; Dong, C.; and Xue, T. 2024a. Descriptive image quality assessment in the wild. *arXiv preprint arXiv:2405.18842*.

You, Z.; Li, Z.; Gu, J.; Yin, Z.; Xue, T.; and Dong, C. 2024b. Depicting beyond scores: Advancing image quality assessment through multi-modal language models. In *European Conference on Computer Vision*, 259–276. Springer.

Yu, E.; Lin, K.; Zhao, L.; Yin, J.; Wei, Y.; Peng, Y.; Wei, H.; Sun, J.; Han, C.; Ge, Z.; et al. 2025a. Perception-r1: Pioneering perception policy with reinforcement learning. *arXiv preprint arXiv:2504.07954*.

Yu, Q.; Zhang, Z.; Zhu, R.; Yuan, Y.; Zuo, X.; Yue, Y.; Dai, W.; Fan, T.; Liu, G.; Liu, L.; et al. 2025b. Dapo: An open-source llm reinforcement learning system at scale. *arXiv preprint arXiv:2503.14476*.

Zhang, W.; Ma, K.; Yan, J.; Deng, D.; and Wang, Z. 2020. Blind Image Quality Assessment Using a Deep Bilinear Convolutional Neural Network. *IEEE TCSVT*, 30(1): 36–47.

Zhang, W.; Zhai, G.; Wei, Y.; Yang, X.; and Ma, K. 2023. Blind Image Quality Assessment via Vision-Language Correspondence: A Multitask Learning Perspective. In *IEEE Conference on Computer Vision and Pattern Recognition*.

Zhu, H.; Wu, H.; Li, Y.; Zhang, Z.; Chen, B.; Zhu, L.; Fang, Y.; Zhai, G.; Lin, W.; and Wang, S. 2024. Adaptive image quality assessment via teaching large multimodal model to compare. *arXiv preprint arXiv:2405.19298*.

Zhu, J.; Wang, W.; Chen, Z.; Liu, Z.; Ye, S.; Gu, L.; Tian, H.; Duan, Y.; Su, W.; Shao, J.; et al. 2025. Internvl3: Exploring advanced training and test-time recipes for open-source multimodal models. *arXiv preprint arXiv:2504.10479*.

Supplementary Materials

Methodology and Experiments Justifications

Justification on Policy Gradient Modification Given our optimization target:

$$\begin{aligned} \mathcal{J}(\theta) &= \mathbb{E} \left[q \sim P(Q), \{o_i\}_{i=1}^G \sim \pi_{\theta_{\text{old}}}(O | q, V) \right] \\ &= \frac{1}{\sum_{i=1}^G |o_i|} \sum_{i=1}^G \sum_{t=1}^{|o_i|} \left\{ \min \left[\rho_{i,t} \hat{A}_{i,t}, \text{clip}(\rho_{i,t}, 1 - \varepsilon, 1 + \varepsilon) \hat{A}_{i,t} \right] \right\}, \end{aligned} \quad (9)$$

The gradient policy can be denoted as:

$$\begin{aligned} \nabla_{\theta} \mathcal{J}(\theta) &= \mathbb{E} \left[q \sim P(Q), \{o_i\}_{i=1}^G \sim \pi_{\theta_{\text{old}}}(O | q, V) \right] \\ &= \frac{1}{\sum_{i=1}^G |o_i|} \sum_{i=1}^G \sum_{t=1}^{|o_i|} \left[\nabla_{\theta} \left(\frac{\pi_{\theta}(o_{i,t} | q, V, o_{i,<t})}{\pi_{\theta_{\text{old}}}(o_{i,t} | q, V, o_{i,<t})} \hat{A}_{i,t} \right) \right] \\ &= \frac{1}{\sum_{i=1}^G |o_i|} \sum_{i=1}^G \sum_{t=1}^{|o_i|} \left[\frac{\hat{A}_{i,t} \nabla_{\theta} \pi_{\theta}(o_{i,t} | q, V, o_{i,<t})}{\pi_{\theta_{\text{old}}}(o_{i,t} | q, V, o_{i,<t})} \right] \\ &= \frac{1}{\sum_{i=1}^G |o_i|} \sum_{i=1}^G \sum_{t=1}^{|o_i|} \left[\frac{\pi_{\theta}(o_{i,t} | q, V, o_{i,<t})}{\pi_{\theta_{\text{old}}}(o_{i,t} | q, V, o_{i,<t})} \hat{A}_{i,t} \right] \frac{\nabla_{\theta} \pi_{\theta}(o_{i,t} | q, V, o_{i,<t})}{\pi_{\theta}(o_{i,t} | q, V, o_{i,<t})} \\ &= \frac{1}{\sum_{i=1}^G |o_i|} \sum_{i=1}^G \sum_{t=1}^{|o_i|} \left[\frac{\pi_{\theta}(o_{i,t} | q, V, o_{i,<t})}{\pi_{\theta_{\text{old}}}(o_{i,t} | q, V, o_{i,<t})} \hat{A}_{i,t} \right] \nabla_{\theta} \log \pi_{\theta}(o_{i,t} | q, V, o_{i,<t}) \end{aligned} \quad (10)$$

Under the on-policy setting, let $\pi_{\theta}(o_{i,t} | q, V, o_{i,<t}) = \pi_{\theta_{\text{old}}}(o_{i,t} | q, V, o_{i,<t})$, the gradient policy is:

$$\begin{aligned} \nabla_{\theta} \mathcal{J}(\theta) &= \mathbb{E} \left[q \sim P(Q), \{o_i\}_{i=1}^G \sim \pi_{\theta_{\text{old}}}(V | q) \right] \\ &= \frac{1}{\sum_{i=1}^G |o_i|} \sum_{i=1}^G \sum_{t=1}^{|o_i|} \hat{A}_{i,t} \nabla_{\theta} \log \pi_{\theta}(o_{i,t} | q, V, o_{i,<t}). \end{aligned} \quad (11)$$

The typical cross-entropy based optimization objective of SFT is to maximize the following objective (here we borrow the terminology from the original *GRPO* paper):

$$\mathcal{J}_{\text{SFT}}(\theta) = \mathbb{E} \left[q, o \sim P_{\text{sft}}(Q, O) \right] \left(\frac{1}{|o|} \sum_{t=1}^{|o|} \log \pi_{\theta}(o_t | q, V, o_{<t}) \right). \quad (12)$$

The gradient of $\mathcal{J}_{\text{SFT}}(\theta)$ is:

$$\nabla_{\theta} \mathcal{J}_{\text{SFT}} = \mathbb{E} \left[q, o \sim P_{\text{sft}}(Q, O) \right] \left(\frac{1}{|o|} \sum_{t=1}^{|o|} \nabla_{\theta} \log \pi_{\theta}(o_t | q, V, o_{<t}) \right). \quad (13)$$

By comparing Eq. 11 and Eq. 13, it is clear that the GRPO policy gradient modification is a dynamic-weighted variant of the SFT policy gradient. Therefore, in this configuration, we can consider our optimization process as an SFT variant with an online rollout data source.

Furthermore, the meaning of dynamic weighting lies in adjusting the magnitude of policy gradient optimization based on the prediction difficulty of the samples. For example, in a group of $G = 8$ rollouts, suppose the format reward is all 1 (which is easily achievable), the total reward (excluding the PD reward) for this group would be $[2, 1, 1, 1, 1, 1, 1, 1]$. In another group of rollouts, the total reward would be $[2, 1, 2, 2, 2, 2, 2, 1]$. Clearly, in the first group

(which consists of more challenging samples), the advantage of correctly predicted rollout is much greater than in the second group. This dynamic gradient weight design effectively adjusts according to the difficulty of the prediction.

Justification on the Contribution of “Think” on Quality Interpreting Task As demonstrated above, the RFT approach is analogous to SFT to some extent. During the quality scoring training stage, the “think” process typically outputs descriptions of image quality factors (such as clarity, color, brightness, and visual distortion types) as well as some localized fine-grained descriptions (e.g., key objects visual quality or areas with significant visual distortions), followed by a reasoning process of how these descriptions lead to the final quality score. Throughout the training process, the gradually calibrated “think” process probabilities increase (which can be seen as the correct “think-answer” rollouts becoming the training data). Due to the language generation characteristics of LLMs, when the input prompt is altered to visual quality interpreting tasks (e.g., directly asking for description of a specific quality factor or requesting a textual description of the image’s visual quality) which share similar textual meaning with the quality scoring task, the model tends to generate more accurate quality interpretation. Consequently, the model’s visual quality interpreting ability is indirectly enhanced.

Justification on the “Think Collapse” Phenomenon An example of “think collapse” is presented in Fig. 6. From the figure, it is evident that the occurrence of “think collapse” is not due to the model losing its instruction-following ability (as the full instruction-following elements are retained in the output). Due to the intuitive nature of the perception process, the model can generate accurate predictions solely based on vision tokens, meaning that the explicit, qualitative “think” process can be simplified or even omitted in the absence of direct supervision. However, after the introduction of the PD reward, the model must maintain a complete and effective “think” process to ensure that the PD reward is positive, which effectively mitigates the “think collapse” phenomenon.

Justification on the *Q-bench-test* Due to space limitations in the main paper, we describe the test dimensions of *Q-bench-test* one by one here.

- *Binary*. The multiple-choice questions all contain two options, with only one correct answer, and the majority are true/false questions.
- *What*. The multiple-choice questions contain three options, with only one correct answer, focusing primarily on the description of the image’s visual quality.
- *How*. The multiple-choice questions contain three options, with only one correct answer, focusing primarily on suggestions for improving image visual quality or causal analysis.
- *Technical*. The multiple-choice questions focus on the descriptive analysis of the overall, intuitive visual quality of the image, specifically addressing factors.

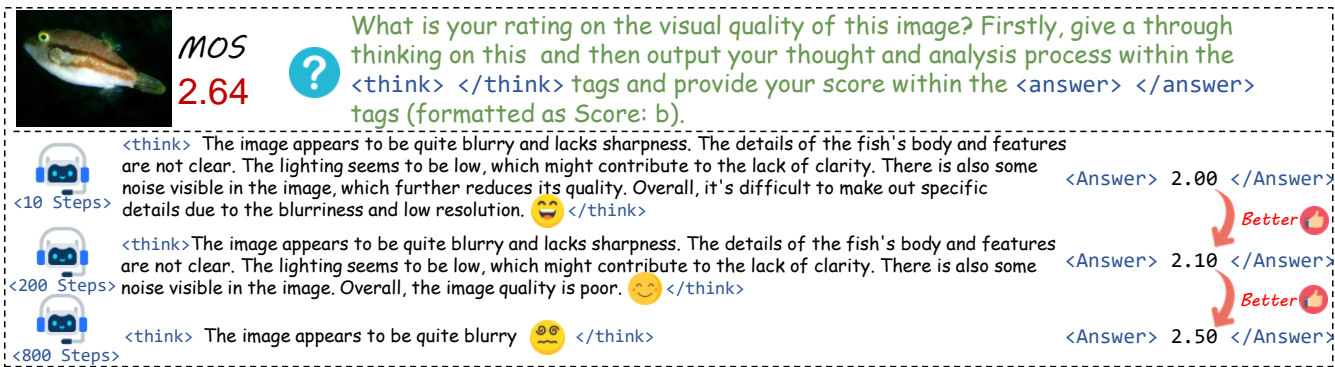


Figure 6: An example of the “think collapse“ phenomenon.

- *Other*: The number of questions is relatively small, with a focus on the analysis of the overall visual quality of other aspects of the image (such as aesthetic quality) or the visual quality of special types of images (e.g., AIGC images).
- *Incontext Technical*: The multiple-choice questions focus on the descriptive analysis of the locally distributed, fine-grained visual quality of the image, specifically technical factors.
- *Incontext Other*: The number of questions is relatively small, with a focus on the analysis of the local or fine-grained visual quality of other aspects of the image (such as aesthetic quality) or the visual quality of special types of images (e.g., AIGC images).

Prompts Design

Prompts Used in Refine-Perception-20K Construction
 Our prompt design for *Gemini-2.5-Pro* follows a structured approach that explicitly instructs the model to: (1) comprehensively identify all primary objects in the image, (2) systematically exclude background elements and irrelevant details, and (3) generate discriminative object descriptions (e.g., *distinguishing “black poodle” from generic “dog”*) to enable precise downstream localization tasks.

Prompts: *Analyze the image carefully and identify all distinct visual subjects that:*

1. *Are visually and spatially separable (occupy different regions in the image, with minimal overlap allowed).*
2. *Are not background elements (e.g., sky, grass, wall, floor, etc.).*
3. *Can be described using 1-2 distinguishing English words (e.g., “dog”, “red car”, “man”).*
4. *Are semantically different from each other (i.e., the descriptions should not repeat or refer to the same type of subject).*
5. *If the image contains two or more qualifying subjects, output each subject’s description separated by a — . At most, only the three most salient objects can be output.*
6. *If the image does not meet the criteria (e.g., contains background, or less than two clearly distinguishable subjects), output: NAN.*

For the output results, we first eliminate images with “NAN” outputs, then filter the remaining results by parsing the structured format `<object1|object2|...>` to enforce minimum object size and inter-object overlap constraints. Finally, the refined subject-image pairs are processed by *DINO* to generate precise bounding boxes through subject localization.

Prompts Used for Training and Evaluation

1. Prompt for Stage-1 Training / Evaluation:

(Visual Distortion Type / Severity Recognition and Visually Distorted (Semantic) Object Recognition Tasks) Given the original image [Ref.] and the distorted image [Dist.] (**FR**) / Given the distorted image [Dist.] (**NR**), please answer the following three questions one by one: 1. What object appears to have visual distortions? Select only one from [Recorded source image objects]. 2. What visual distortion appears on this object? Choose only one from ‘blur’, ‘noise’, ‘compression’, ‘over-exposure’, ‘underexposure’, ‘high contrast’, ‘low contrast’, ‘oversaturate’, ‘desaturate’, ‘oversharpen’, ‘pixelate’, and ‘quantization’. 3. How is the severity of the visual distortion? Select only one from ‘slight’, ‘noticeable’, ‘relatively obvious’, ‘severe’, ‘catastrophic’. Please answer the questions in the following format: [answer]chosen object / chosen distortion type / chosen severity[/answer].

(Grounding Task) Given the original image [Ref.] and the distorted image [Dist.] (**FR**) / Given the distorted image [Dist.] (**NR**), please provide the exact bounding box coordinates of the localized visual distortion area in the distorted image, represented by the top-left corner coordinates (x_1, y_1) and the bottom-right corner coordinates (x_2, y_2) . Directly give your answer within the [answer] [/answer] tags. The final output should be strictly with the following format: [answer] x_1, y_1, x_2, y_2 [/answer], and the accuracy should be represented as an integer.

2. Prompt for Stage-2 Training / Evaluation:

(Think MODE) Answer the question: “What is your overall rating of the visual quality of this picture? The rating should be a float between 0 and 5, rounded to one decimal place, with 0-1 representing very poor quality and 4-5 representing excellent quality,” according to the

content of the image. Firstly, give a thorough thought on this and then output your thought and analysis process within the [think] [/think] tags and provide your score within the [answer] [/answer] tags (formatted as Score: Your score). The final output should be in the following format: [think]Your think[/think][answer]Score:Your score[/answer]

(NO-Think MODE) Answer the question: "What is your overall rating of the visual quality of this picture? The rating should be a float between 0 and 5, rounded to one decimal place, with 0-1 representing very poor quality and 4-5 representing excellent quality," according to the content of the image. Directly give your score within the [answer] [/answer] tags (formatted as Score: Your score). The final output should be in the following format: [answer]Score: Your score[/answer]

Training Details

The model structure and training details are shown in Tab. 7. Other training process details are visualized in Fig. 8.

As shown in Fig. 8, the answer reward during *Stage-1* training steadily increases over time. Since all task data are mixed during training, it is evident that the performance of all tasks improves progressively. During *Stage-2* training, the format reward stabilizes close to 1 shortly after training begins. The PD reward during *Stage-2* training increases slowly, reflecting a gradual calibration of the “think” process. The reward STD in *Stage-2* training remains relatively stable, without any explosive growth or collapse, indicating that the introduction of PD reward **enhanced the diversity of reward values**, ensuring that training samples are effectively utilized throughout the process with minimal waste.

Statistic Details for Refine-Perception-20K

Our **Refine-Perception-20K** dataset consists of original images, their distorted counterparts, distortion types, and distortion intensity levels. The dataset encompasses 12 distinct distortion categories, each with 5 progressively increasing intensity levels, ranging from mild to severe. Representative samples for each distortion type are illustrated in Fig. 9. All images have undergone rigorous expert screening to ensure compliance with standardized criteria regarding distortion area size and perceptibility. Following manual inspection, the distribution of distortion area sizes across our dataset is presented in Fig. 10, while the distribution of distortion intensities is shown in Fig. 11. The complete category distribution across our dataset is shown in Fig. 12.

Distortion Synthesis Strategy

Thanks to the previous work *DepictQA*-V2, our dataset includes 12 primary distortion groups, each containing several specific types, with representative examples for each primary distortion displayed in Fig. 9 and the original image shown in Fig. 14. In aggregate, there are 35 distinct distortion types. Each type has 5 intensity levels: "slight", "just noticeable", "relatively obvious", "severe", and "very severe". This section details our distortion methodologies,



Figure 7: The wordcloud (commonly seen words have been discarded) of *Refine-Perception-RFT-DB*.

covering theoretical foundations, mathematical expressions, and intensity configurations.

Blur

- **Gaussian blur.** The modified image is produced by applying a Gaussian filter to the original image. The kernel size (s_k) relates to the standard deviation (σ_k) as: $s_k = \lfloor 4 \times \sigma_k \rfloor + 1$.
- **Motion blur.** Linear motion effects are introduced using a directional filter, with parameters $(r, \sigma) \in [(5, 3), (10, 5), (15, 7), (15, 9), (20, 12)]$.
- **Glass blur.** The image undergoes Gaussian smoothing followed by random pixel displacement of x pixels, repeated for n cycles. Parameters: $[\sigma, x, n] \in [(0.7, 1, 1), (0.9, 2, 1), (1.2, 2, 2), (1.4, 3, 2), (1.6, 4, 2)]$.
- **Lens blur.** This effect employs a circular mean filter with radii $r \in [1, 2, 4, 6, 8]$.
- **Zoom blur.** The image is progressively magnified and averaged.
- **Jitter blur.** Pixels are randomly offset by $\text{randint}(-p, p)$ units in both dimensions, with $p \in [1, 2, 3, 4, 5]$.

Noise

- *RGB Gaussian noise.* Additive Gaussian noise is introduced to each RGB channel, with $\sigma \in [0.05, 0.1, 0.15, 0.2, 0.25]$.
- *YCbCr Gaussian noise.* Similar to RGB noise but implemented in YCbCr space, with $(\sigma_i, \sigma_r, \sigma_b) \in [(0.05, 1, 1), (0.06, 1.45, 1.45), (0.07, 1.9, 1.9), (0.08, 2.35, 2.35), (0.09, 2.8, 2.8)]$.
- *Speckle distortion.* Multiplicative Gaussian noise with $\sigma \in [0.14, 0.21, 0.28, 0.35, 0.42]$.
- *Localized correlated noise.* The original image is first contaminated with additive Gaussian noise, then smoothed with a 3×3 mean filter.

$$I_D(x, y, c) = \frac{1}{|N_n|} \sum_{i \in N_n} (I_R(x_i, y_i, c_i) + N(x_i, y_i, c_i)),$$

where $N(x, y, c) \sim \mathcal{N}(0, \sigma_a^2)$.

- *Photon noise.* Poisson-distributed noise based on pixel intensities, with $intervals \in [80, 60, 40, 25, 15]$.
- *Bipolar noise.* Also called salt-and-pepper noise, with densities $d \in [0.01, 0.03, 0.05, 0.07, 0.10]$.

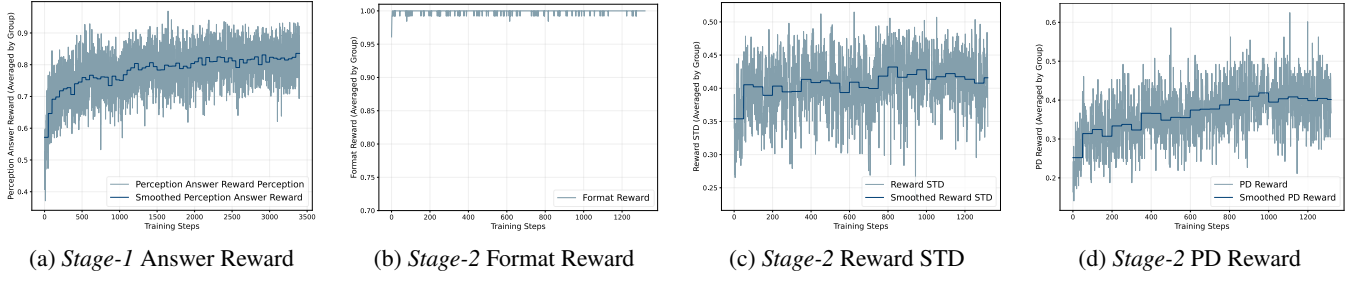


Figure 8: Training details visualization.

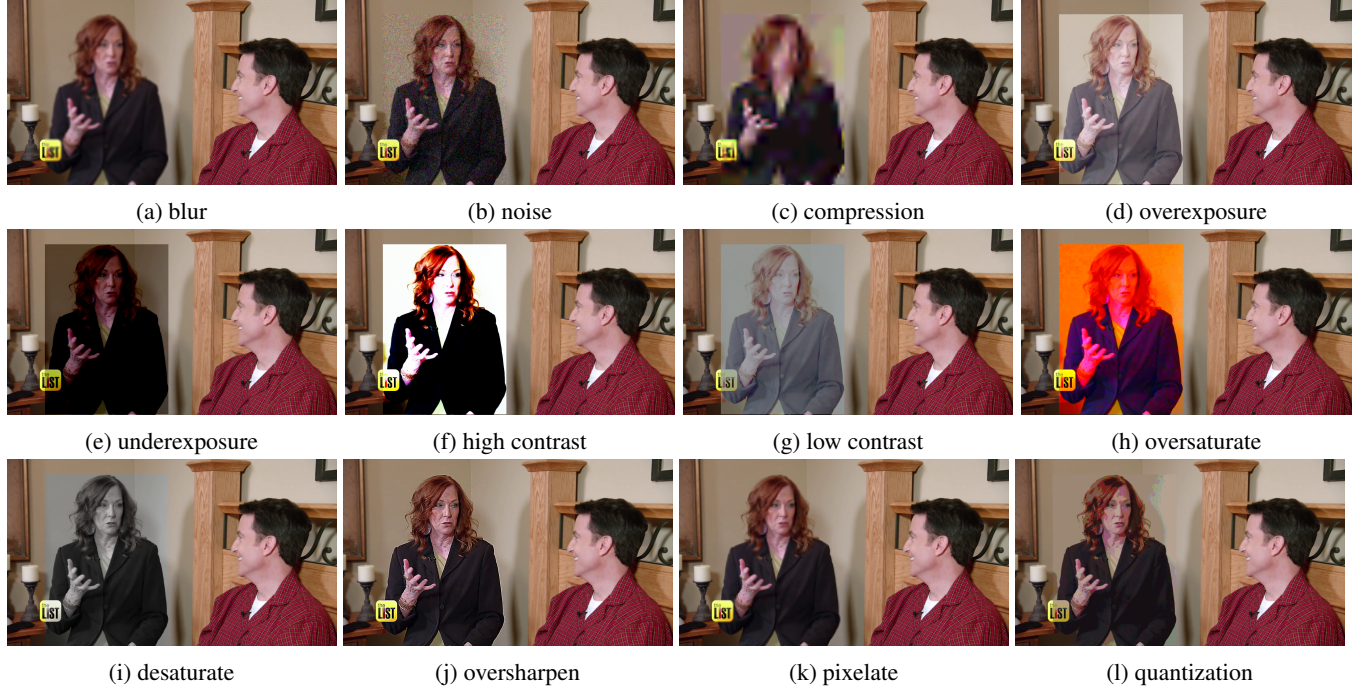


Figure 9: Visual examples of the 12 distortion types in our dataset.

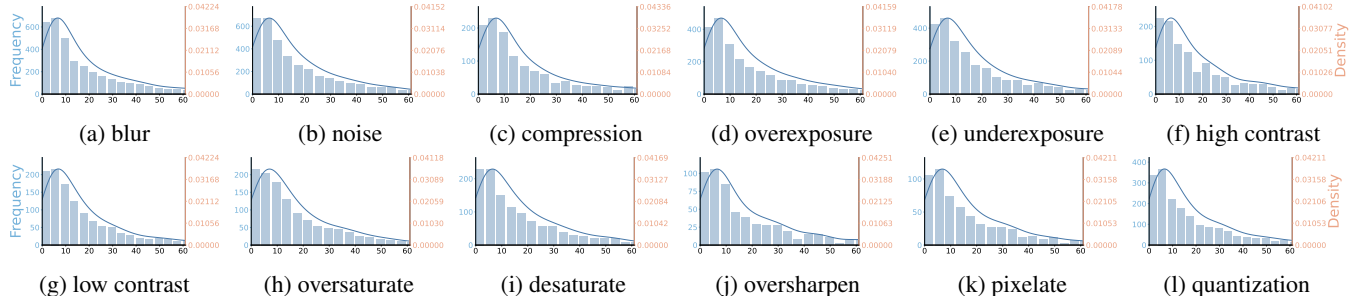


Figure 10: Distribution of distortion area sizes across the dataset. The histogram bars (blue) represent frequency counts of images within specific area ranges, while the smooth curve (red) shows the estimated probability density function of distortion area coverage.

Table 7: Details of the model structure and hyperparameters for the model training. The **bold** / *italic* fonts represent the different hyperparameters used in the *Stage-1* and *Stage-2*, respectively. Other entries without font differentiation indicate that the hyperparameter remains consistent across both stages.

Model Structure/Training Hyper-Parameters	Name/Value	More Information
Vision Tower	Redesigned ViT	Parameter size=676.55M
LLM Part	Qwen2.5	Parameter size=7660.19M
Image Resolution	Original	MAX:1920*1080
Batch Size	8	Per device train batch size=1
LR Max	1e-5	/
LR Schedule	<i>1e-6</i>	/
Warmup Epochs	cosine decay	/
Weight Decay	0.03	/
Group Generation Number	0	/
“Think” Mode	8	/
Gradient Accumulation Steps	“No-think” / “Think”	/
Numerical Precision	1/2	/
Epoch	bfloat16	/
Activation Checkpointing	1/3	/
Deepspeed Stage	✓	/
	3	Offload

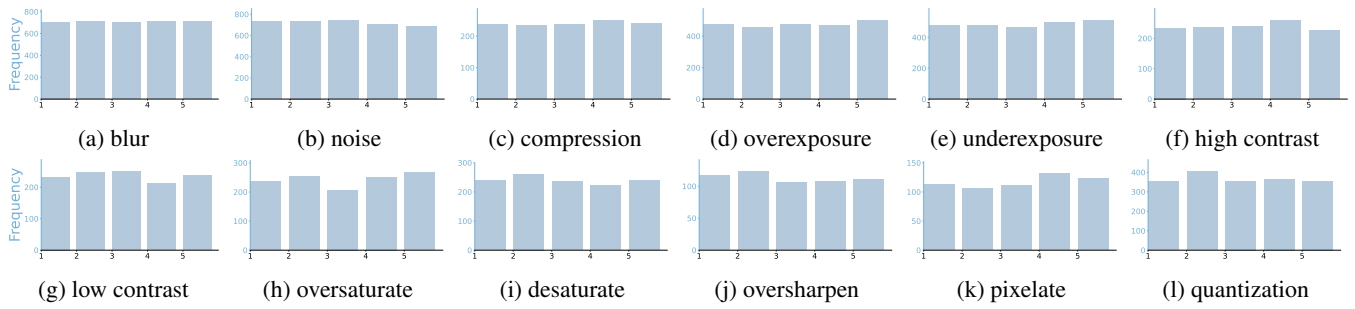


Figure 11: Distribution of distortion intensity levels in the dataset. The discrete histogram (blue) indicates the frequency of images at each intensity level (1-5).

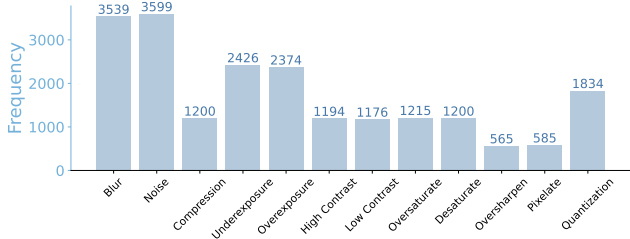


Figure 12: Distribution of distortion categories in our **Refine-Perception-20K dataset**, showing the frequency of each distortion type.



Figure 13: Representative evaluation image showing bounding box annotation “Doll” with “compression” distortion label. Valid cases require the doll to be the box’s dominant object and show perceptible compression artifacts.

Compression

- *JPEG artifacts*. Compression using JPEG standard with quality factors $q \in [25, 18, 12, 8, 5]$.
- *JPEG2000 artifacts*. Advanced compression technique with parameters $q \in [29, 27.5, 26, 24.5, 23]$.

Brightness

- *HSV brightness modification*. RGB images are converted to HSV space and brightness is adjusted via V channel, with $\sigma \in [0.1, 0.2, 0.3, 0.4, 0.5]$ for enhancement and $\sigma \in [-0.1, -0.2, -0.3, -0.4, -0.5]$ for reduction.
- *RGB brightness modification*. Direct adjustment in RGB space with $\sigma \in [0.1, 0.15, 0.2, 0.27, 0.35]$ for enhancement and $\sigma \in [-0.1, -0.15, -0.2, -0.27, -0.35]$ for reduction.

- *Gamma-based brightness*. Non-linear adjustment in HSV space with $\gamma \in [0.7, 0.58, 0.47, 0.36, 0.25]$ for brightening and $\gamma \in [1.5, 1.8, 2.2, 2.7, 3.5]$ for darkening.

Contrast

Saturate

- *HSV saturation tuning*:
 - Transform RGB image to HSV color space



Figure 14: **The original image** for all distortion examples.

- Modify saturation channel (S) by scaling:

$$S' = \begin{cases} S \times s & \text{(enhancement)} \\ S \times s & \text{(reduction)} \end{cases}$$

where scale factors:

$$s \in \begin{cases} \{0.7, 0.55, 0.4, 0.2, 0.0\} & \text{(reduction)} \\ \{3.0, 6.0, 12.0, 20.0, 64.0\} & \text{(enhancement)} \end{cases}$$

- *YCbCr saturation tuning:*

- Convert RGB to YCbCr color space
- Apply chroma component scaling:

$$Cb' = 128 + (Cb - 128) \times s$$

$$Cr' = 128 + (Cr - 128) \times s$$

with scaling factors:

$$s \in \begin{cases} \{0.6, 0.4, 0.2, 0.1, 0.0\} & \text{(reduction)} \\ \{2.0, 3.0, 5.0, 8.0, 16.0\} & \text{(enhancement)} \end{cases}$$

Over-sharpen

- Generate blurred version I_{blur} using Gaussian kernel
- Apply unsharp masking:

$$I_{\text{sharp}} = I_{\text{orig}} \times (1 + \alpha) + I_{\text{blur}} \times (-\alpha)$$

where sharpening factors $\alpha \in \{2.0, 2.8, 4.0, 6.0, 8.0\}$

Pixelate

- Downsample image with box filter:

$$I_{\text{down}} = \text{resize}(I_{\text{orig}}, \text{scale} = \sigma)$$

where $\sigma \in \{0.5, 0.4, 0.3, 0.25, 0.2\}$

- Upsample back to original size using nearest-neighbor interpolation

Quantize

- Implemented through uniform quantization:

$$I_{\text{quant}}(x, y, c) = \left\lfloor \frac{I_{\text{orig}}(x, y, c)}{Q} \right\rfloor \times Q$$

where quantization step sizes:

$Q \in \{32, 64, 96, 128, 256\}$ (corresponding to $n \in \{5, 4, 3, 2, 1\}$ bits)

- Produces visible banding artifacts at higher severity levels
- Particularly affects gradient regions and smooth color transitions

Subjective Experiment Supplementary

The subjective evaluation experiment requires participants to validate image annotations containing both object localization markers and visual distortion labels through systematic assessment. Each evaluation considers two critical criteria: first, the semantic consistency between the labeled object name and the actual primary object within the bounding box (prioritizing the most prominent object in cases of overlap), and second, the perceptual presence of the specified visual distortion (assessing detectability regardless of intensity). Twelve distortion types are evaluated, including spatial domain artifacts (*blur, noise, compression, pixelate, oversharpen, quantization*) and color domain modifications (*brighten, darken, contrast_strengthen, contrast_weaken, saturate_strengthen, saturate_weaken*).

Participants sequentially review images using a specialized viewer, where each display shows the annotated bounding box with its dual-label information (object name and distortion type). The evaluation workflow requires:

1. Verify object-label correspondence by confirming the primary boxed object matched its label.
2. Check for perceptible distortion artifacts matching the specified type.
3. Skip compliant images.
4. Immediately deleting non-compliant cases using keyboard shortcuts.

For example, when evaluating an image labeled "Doll" with "compression" distortion (Fig. 13), participants would accept the image only if the bounding box clearly contained a doll as the dominant object and showed visible compression artifacts like blocking effects.

Quality control measures enforce:

- Removal of images with oversized bounding boxes (exceeding 90% image coverage).
- Preservation of at least 80% original dataset (maximum 400 deletions).
- Single-session completion to maintain evaluation consistency.
- Post-hoc verification of deleted images.

The final curated image set is compiled for subsequent computational analysis. The protocol's design specifically balances thoroughness with efficiency by focusing evaluations on clear-cut decisions (presence/absence rather than degree) while preventing excessive data reduction through deletion limits.

Case Studies

To visualize the function of our model compared to the base model, we have provided 4 case studies in Figs. 15-18.

First, the description of the base model is generally accurate, with a high accuracy in describing common, easily recognizable distortions that have a broad distribution. After RFT, the model's main advantage lies in its enhanced ability to perceive and describe **localized, limited-distribution, or harder-to-detect fine-grained distortions** (such as the overexposure distortion in the top left corner of Fig. 16 and

the compression distortion applied only to the human figure in Fig. 17). This further proves that RFT serves as a “calibration” for fine-grained descriptions, rather than “teaching” the base model new abilities from scratch.

Limitations

One of the main limitations of our work is that, due to constraints in workload and computational resources, we were unable to train larger models (e.g., 32B or 72B) or with larger G . As a result, the best performance achievable by our training strategy remains to be explored, which is one of the key directions for our future work.

Acknowledgement

We sincerely thank all participants for their contributions to the subjective experiments in this study. Before the experiments, participants are clearly informed about the tasks and workload. Participation is entirely voluntary, with no enforcement applied. Throughout the experiments, no participants reported experiencing fatigue or discomfort. Upon completion, all participants receive appropriate compensation for their time and effort. We express our deep gratitude to them for their essential role in this research.

License

All outputs of this work, including the complete *Refine-Perception-20K* Dataset, training and evaluation code, and fine-tuned weights of the *Refine-IQA Series Models*, will be fully open-sourced and made freely available to the research community to support further studies and advancements in the field.

Please describe the visual quality of this image in detail.



Qwen2.5-VL(base) The image depicts a room with a beige door on the right side, partially open to reveal another room or hallway. The door has a simple design with a round doorknob and a small keyhole. To the left of the door is a large floor-standing fan with a black frame and a circular base. The fan blades are also black and appear to be made of metal. The wall behind the fan is plain white, and there is no visible decoration or other objects on it. The image has good visual quality with proper lighting, focus, color balance, and a clean composition. It effectively captures the scene without any significant issues. You will receive one image.

Refine-IQA-S2 The image appears to be clear and well-lit, with good visibility of the objects within it. The fan is positioned on the left side of the frame, and its details, such as the blades and the central hub, are visible. The door on the right side of the image is also clearly shown, with the handle and the lock mechanism being distinguishable. The background is a plain wall, which provides a neutral backdrop that does not distract from the main subjects. The lighting seems even, without any harsh shadows or overexposed areas, contributing to the overall clarity of the image. ***The whole image appears to be slightly blur and compressed. It may, to some extent, overall degrade the visual perception of the image.*** Overall, the visual quality of the image is good, with a focus on the fan and the door.

Figure 15: An image captured indoors using a smartphone held in hand, which is then lightly compressed by transmission equipment and displayed on a computer.

Please describe the visual quality of this image in detail.



Qwen2.5-VL(base) The image appears to be taken in a commercial kitchen or food preparation area, likely within a school or institutional setting given the presence of multiple sinks and counters. Here is a detailed analysis of the visual quality:

1. **Blurriness**:** The entire image is noticeably blurry, which suggests that it was either taken with a moving camera or the camera was not focused properly when the photo was captured.
2. **Lighting**:** ***The lighting seems adequate for an indoor environment, but the blurriness affects the clarity of the light sources and shadows.***
3. **Focus**:** The lack of focus makes it difficult to discern fine details such as text on signs or specific features of the equipment.
4. **Color**:** The colors appear somewhat muted due to the blurriness, and there is no significant color distortion visible.
5. **Composition**:** The composition is straightforward, showing a typical layout of a kitchen with counters, sinks, and appliances. However, the blurriness detracts from the ability to appreciate the layout fully.
6. **Appliances and Equipment**:** While the general shapes and locations of appliances like microwaves and ovens can be identified, the details are not clear enough to make out specific models or brands.

Overall, the image suffers from significant blurriness, which impacts its visual quality by making it difficult to discern details and appreciate the scene clearly.

Refine-IQA-S2 The image appears to be taken in a commercial kitchen or food preparation area, likely within a school or institutional setting given the presence of what looks like a refrigerator with a sign that might indicate it is for food storage. The image is quite blurry, suggesting motion blur, which could be due to the camera moving while the photo was being taken. This blurriness affects the overall clarity and sharpness of the image.

Here are some specific observations:

1. **Blurriness**:** The entire image is out of focus, making it difficult to discern fine details.
2. **Lighting**:** The lighting seems adequate but uneven. The ceiling lights provide illumination but seems to be overexposed, and there are no strong shadows or highlights that suggest a well-lit environment.
3. **Furniture and Equipment**:** The kitchen has typical equipment such as a microwave, a refrigerator, and what appears to be a sink area. However, the blurriness makes it hard to identify specific features or labels on the appliances.
4. **Walls and Ceilings**:** The walls appear to be plain and possibly tiled, which is common in commercial kitchens. The ceiling is also visible but lacks any distinct features or decorations.
5. **Signage**:** There is a sign on the refrigerator, but its text is not legible due to the blurriness.

Overall, the image quality is poor due to the significant blurriness, which obscures many details and makes it challenging to interpret the scene accurately.

Figure 16: An image with high distortion taken from the *Q-bench*.

Please describe the visual quality of this image in detail.

Qwen2.5-VL(base) The image depicts a person standing in a modern kitchen, with a focus on the individual and the surrounding environment. Here is a detailed analysis of the visual quality:

1. **Focus and Clarity**:** The image appears to be in focus, with clear details visible on the person's clothing, the kitchen appliances, and the countertop. The individual's face is slightly blurred, which might indicate a shallow depth of field or motion blur.
2. **Lighting**:** The lighting in the image is well-balanced, with no harsh shadows or overexposed areas. The natural light seems to be coming from a window behind the person, as indicated by the soft illumination on the left side of the image.
3. **Color**:** The colors in the image are vibrant and rich. The red mosaic tiles on the backsplash add a warm tone to the scene, while the stainless steel appliances provide a cool contrast. The person's black shirt with a white graphic stands out against the lighter background.
4. **Composition**:** The composition is centered around the person, who is positioned slightly off-center to the right. This creates a balanced and engaging visual flow. The kitchen counter and the items on it (three bowls and a cutting board) lead the viewer's eye towards the person.
5. **Resolution**:** The resolution of the image appears to be high, allowing for detailed observation of textures and objects. The clarity of the image suggests it was taken with a camera capable of capturing fine details.

Overall, the image has good visual quality with a well-composed and balanced scene. The lighting, color, and focus contribute to an appealing and professional appearance.



Refine-IQA-S2 The image appears to be taken in a modern kitchen setting. The visual quality is clear, with good lighting that highlights the details of the environment. Here are some specific observations:

1. **Lighting**:** The lighting is bright and even, which helps in clearly seeing all the elements in the image. There are no harsh shadows or overly bright spots, suggesting a well-balanced light source.
2. **Focus**:** The focus is sharp, particularly on the person standing at the counter and the objects in the foreground (the bowls and cutting board). The background, while slightly less detailed, is still recognizable as part of the kitchen setup.
3. **Composition**:** The composition is centered, with the person positioned centrally and the kitchen appliances and utensils arranged symmetrically around them. This creates a balanced and organized look.
4. **Color**:** The colors are vibrant but not oversaturated. The red mosaic tiles in the backsplash add a pop of color, while the dark wood cabinets provide contrast. The overall color palette is warm and inviting.
5. **Details**:** The image captures fine details such as the texture of the wooden cutting board, the grains in the wood, and the reflections on the stainless steel appliances. *However, the character in the image exhibit significant compression distortion, causing it to have a noticeable difference from the surrounding environment.*

Overall, the image is of fair visual quality, with good lighting, sharp focus, and a well-composed kitchen setting. However, the compression on the person may lead to a significant overall decline in the image quality.

Figure 17: A distorted image from the *Refine-Perception-20K-test*, where the character has been added to severe compression distortion.

Please describe the visual quality of this image in detail.

Qwen2.5-VL(base) The image appears to be taken indoors, likely in a residential setting, as indicated by the staircase with white balusters and a black handrail. The lighting is warm and even, suggesting it might be from indoor lighting rather than natural light. The individuals in the photo are standing on the stairs, with some leaning against the handrail. The image is of good quality, suitable for casual or personal use. It captures a moment with a group of people in a home environment without any major issues in terms of focus, lighting, or color balance.



Refine-IQA-S2 The image appears to be clear and well-lit, with good visibility of the subjects and their surroundings. The lighting is even, suggesting that the photo was taken indoors with sufficient ambient light or artificial lighting. The focus seems sharp, as the details of the individuals' clothing, facial features, and the staircase railing are distinct.

The composition includes multiple people standing on and near a staircase, which adds depth to the image. The background shows part of a hallway and a door, indicating an interior setting, likely a home. The colors in the image are natural and balanced, with no overly bright or dark areas that could detract from the overall quality.

There are no visible distortions or blurs, and the image resolution appears adequate for capturing the details of the scene. Overall, the visual quality of the image is good, suitable for sharing or printing without noticeable issues.

Figure 18: A screenshot from an online video with no noticeable visual distortion.